

Distance and Kinematics of the TW Hydrae Association from Parallaxes

Alycia J. Weinberger

Department of Terrestrial Magnetism, Carnegie Institution of Washington

5241 Broad Branch Road NW, Washington, DC 20015

`weinberger@dtm.ciw.edu`

Guillem Anglada-Escudé

Universität Göttingen, Institut für Astrophysik

Friedrich-Hund-Platz 1, 37077 Göttingen, Germany

Alan P. Boss

Department of Terrestrial Magnetism, Carnegie Institution of Washington

5241 Broad Branch Road NW, Washington, DC 20015

ABSTRACT

From common proper motion and signatures of youth, researchers have identified about 30 members of a putative TW Hydrae Association. Only four of these had parallactic distances from Hipparcos. We have measured parallaxes and proper motions for 14 primary members. We combine these with literature values of radial velocities to show that the Galactic space motions of the stars, with the exception of TWA 9 and 22, are parallel and do not indicate convergence at a common formation point sometime in the last few million years. The space motions of TWA 9 and 22 do not agree with the others and indicate that they are not TWA members. The median parallax is 18 mas or 56 pc. We further analyze the stars' absolute magnitudes on pre-main sequence evolutionary tracks and find a range of ages with a median of 10.1 Myr and no correlation between age and Galactic location. The TWA stars may have formed from an extended and filamentary molecular cloud but are not necessarily precisely coeval.

Subject headings: open clusters and associations: individual (TW Hydrae) – stars: distances – stars: kinematics and dynamics – stars: pre-main sequence

1. Introduction

Nearby young stars of age ~ 5 –10 Myr provide our best opportunity to study the late stages of star and planet formation with high sensitivity and spatial resolution. During this time period, the last gas-rich disks dissipate, and the onset of the debris disk phase occurs. The star TW Hydrae sports a massive disk and was first identified as an isolated T Tauri star (Rucinski & Krautter 1983)

and then the first member of an association of young stars (de la Reza et al. 1989; Gregorio-Hetem et al. 1992; Kastner et al. 1997). As the nearest example of a protoplanetary disk, TW Hya has been studied at every available wavelength and spatial resolution, but to understand its disk in context, TW Hya’s age must be well-determined and its disk evolution compared to other stars of similar age and mass.

Over the last decade, ~ 30 members of a putative TW Hydrae Association (TWA) have been identified from a combination of stellar-activity searches and space motion studies (e.g. Webb et al. 1999; Sterzik et al. 1999; Zuckerman et al. 2001; Gizis 2002; Song et al. 2003; Scholz et al. 2005; Loofer et al. 2007; Shkolnik et al. 2011). Members range in spectral type from A0 to brown dwarfs and have presumed common ages ~ 10 Myr, as determined from Li depletion and modeling on pre-main sequence evolutionary tracks (Barrado Y Navascués 2006). Disks in TWA range from the four accreting, gas rich, protoplanetary ones (TWA 1, 3, 27, and 30), to seven transitional or debris disks (TWA 4B, 7, 11A, 26, 28, 31 and 32), to the majority of members that have no detectable disks at all (Weinberger et al. 2004; Low et al. 2005; Riaz & Gizis 2008; Plavchan et al. 2009; Schneider et al. 2012).

The Hipparcos mission determined distances to only four TWA members, including TW Hya itself, for an average distance of 70 pc. Although the association contains the youngest stars close to the Sun, most of its members are low-mass stars and were therefore too faint for Hipparcos. Ground-based parallaxes have been measured for two brown dwarfs in the association – TWA 27 (2M1207) (Gizis et al. 2007) and TWA 28 (SSSPM J1102) (Teixeira et al. 2008), and one additional star that may not actually be a member – TWA 22AB, (Teixeira et al. 2009). This highlights the problem of determining association membership – although their proper motions are similar, as ensured by search methods, without distances and therefore true Galactic space motions TWA stars can only be presumed to be associated. Hence, various members have been suggested and then excluded by proper motion studies using varyingly restrictive conditions for membership (e.g. Makarov & Fabricius 2001; Song et al. 2003; Mamajek 2005).

Distances to a substantial number of members would aid in defining the association and estimating its age from pre-main sequence tracks. If the kinematics allow, a cluster expansion age could also be determined. In this paper we present parallaxes and proper motions to 14 primary stars and two visual binary companions.

2. Data

We have observed 14 TWA primary members with the CAPSCam instrument at the 2.5m DuPont Telescope at Las Campanas Observatory. The instrument and basic data reduction techniques are described in Boss et al. (2009) and Anglada-Escudé et al. (2012) and only briefly summarized here. CAPSCam utilizes a Hawaii-2RG HyViSI detector filtered to a bandpass of 100 nm centered at 865 nm with 2048x2048 pixels, each subtending $0''.196$ on a side. The main advantage of this camera is its ability to achieve simultaneously high S/N on a bright target star and fainter astrometric reference stars. Our typical TWA sources have $I \approx 10$ (see Table 1); we place these bright target stars in an independently readable subarray called the “guide window” (GW). We typically

locate the GW in the center of the full field (FF) and rapidly read and reset it for integration times down to 0.2 s for a 64×64 pixel subarray. Simultaneously, the FF integrates for as long as necessary to obtain high S/N on many reference stars. Table 1 gives typical integration times for each target in the GW and FF, although the times were adjusted during each epoch to account for seeing and clouds.

We drew our sample from stars without parallaxes (thus excluding TWA 1, 4AB, 9AB, 11A, 22, 27, and 28). We only observed bona fide members identified in the convergent point analysis of Mamajek (2005); thus we excluded TWA 17, 18, 19AB, and 24. Although Mamajek (2005) exclude TWA 12, we included it because of its large discrepancy between photometric (Song et al. 2003) and kinematic distance. We excluded TWA 3AB for being too bright. CAPSCam saturates in 0.2 s on $I \approx 9$. We excluded TWA 6, 7, and 11B for being near very bright stars that would fall within the CAPSCam field of view because saturated images leave long-lasting after-images on the detector. We excluded TWA 8AB because the two stars, separated by $13''$ do not fit in the 64×64 GW. Three targets – 30AB, 31, and 32, were discovered after our survey began (Looper et al. 2010; Shkolnik et al. 2011). The remaining stars were all observed with the exception of TWA 10 (Table 1). CAPSCam could in the future provide parallaxes for the remaining stars with $I > 9$ – TWA 8AB, 10, 17, 18, 30, 31 and 32.

We can operate in a mode, called “Guide-window shutter” (GWS) where an iris shutter opens over the FF only when the GW is integrating and closes during the initial pixel resets and during each GW read. This is done to guarantee that the images in the GW and FF sample the atmosphere identically and that no astrometric bias is introduced between them. Some of our data were taken with the shutter in this mode, but some were taken with no shutter (NS) and some in a mode where the shutter closes during the initial pixel resets but remains open during each GW read (NGWS). In principle, the best astrometric precision is obtained in GWS mode, but we operated without it in order to improve efficiency.

Flat field images to correct for pixel-to-pixel variations either intrinsic to the detector or due to the finite opening time of the iris shutter are obtained while exposing on a quartz lamp projected on a flat-field screen.

The imaging of each astrometric field is repeated typically 15-20 times at each epoch. For each FF image, we obtain many GW images. In post-processing, these are summed and re-inserted into the FF image. For each night, one image is selected as an astrometric template of the field for that night. Sources are found automatically, and a fine centroiding algorithm is applied to produce a catalog with the sub-pixel positions of all of the objects in all of the images of the field for a given night.

Each star was observed in at least four independent epochs, with all but one star observed in five or more, i.e. dates separated by enough days that they provide independent constraints on the parallax. The dates of observation are given in Table 1. Data from all epochs are combined in an astrometric solution to derive the positions, proper motions, and parallaxes of all the stars in each target field. The astrometric solution is an iterative process. An initial catalog of positions is generated from a chosen epoch, a transformation is applied to every other epoch’s catalog to match the initial catalog, and the apparent trajectory of each star is then fitted to a basic astrometric

model. The initial catalog is updated with new positions, proper motions, and parallaxes, and a subset of well-behaved stars is selected to be used as the reference frame. The reference stars must be successfully extracted in every epoch and a subset of at least 15, and more typically 30, are chosen that show the smallest epoch-to-epoch variation in their solutions. Over all of our target fields, these stars have typical I-band magnitudes of 13.5 – 17.9 with a median of 16.2. This process is then iterated a small number of times. Again, details may be found in Anglada-Escudé et al. (2012).

2.1. Zero-Point Parallax Correction

The motion of the target star is measured with respect to background stars, which are not truly stationary and that all have parallactic motions given by the Earth’s motion and therefore move in the same direction. This introduces a small bias, so the average parallax of the reference stars must be removed to find the absolute parallax.

If all the stars in the field had perfectly known distances and that information was inserted a priori, the parallax zero-point correction would always be a positive number. Note, however, that some zero-point corrections in Table 2 are negative. Because we do not know the distances a priori, in the astrometric solution, the parallaxes for all objects are initialized to zero. In the iterations that follow, each individual parallax and proper motion is adjusted. While the mean parallax measurement over all the stars after the first iteration should still be approximately zero, the mean parallax of a subset of them, i.e. those used as reference stars, can be either positive or negative due to statistical fluctuations. At any epoch, the position of a star has centroiding uncertainties, and for distant stars, proper motion will take out all apparent motion of the star leaving positional residuals that are both positive and negative. Therefore, although the true parallax to every star must be positive, we allow the fit parallaxes to take on positive and negative values. The quality of the final astrometric solution as measured by the residuals on all the stars is independent of the value of the mean zero-point parallax and will not be adjusted in subsequent iterations.

To find the zero-point for each field, we estimate a photometric distance to the brightest reference stars by fitting a Kurucz stellar model to catalogued USNO-B1 – B2, R2, and I; (Monet et al. 2003) and 2MASS – J, H, and K_s (Skrutskie et al. 2006) photometry and assuming each star is a dwarf. Giant stars are then easily recognizable because they appear to be so close that they should have detectable parallaxes, and we refit them as giants. Dwarf stars with fit $T_{\text{eff}} < 3800$ K are not considered because the stellar models are less reliable. We average the difference between our astrometrically determined (even if they are not statistically significant) and photometric parallaxes to find the average bias and its uncertainty and subtract it from our relative parallaxes and propagate the uncertainty. A comparison of our parallaxes determined this way to literature values is given in Anglada-Escudé et al. (2012).

In principle, this zero-point correction could be done for the proper motions as well, but the reference stars do not generally have catalogued proper motions to use in measuring their bias. Instead, we estimate our bias directly by comparing the proper motions of the TWA stars themselves as computed from our astrometry with their cataloged values in UCAC3 (Zacharias et al. 2009).

Given that the brightnesses and spectral types of the reference stars have approximately the same distribution for all our targets, which are also in the same general direction in the Galaxy, we can then find a correction of our CAPSCam proper motions to absolute proper motions. Leaving out TWA 13 and 15, which are visual binary stars whose proper motions in the UCAC3 are suspect, ten of our 14 stars have UCAC3 proper motions. CAPSCam-determined proper motions are indeed well correlated with the UCAC3 values, with a mean offset of -8.8 ± 5.5 mas/yr in RA and 1.1 ± 5.1 mas/yr in DEC (Figure 1). We correct these biases to find the proper motions of TWA sources without UCAC3 measurements, i.e. TWA 13AB, 15AB, 26, and 29.

3. Results

The results of our parallax survey are presented in Table 2, including the relative proper motions and parallaxes from the iterative solution, as well as the estimates of zero-point parallax in each field and the resulting absolute parallaxes.

Two targets, TWA 13 and TWA 15, are visual binaries for which we obtained independent astrometry for the two stars in each system. Their solutions agree within their uncertainties.

3.1. Notes on Individual Sources

3.1.1. TWA 5

TWA 5 (i.e. TWA 5A) has a companion brown dwarf (BD) TWA 5B (Webb et al. 1999). It is visible in CAPSCam images taken during good seeing (Figure 2), but the BD is faint enough and widely separated enough that it does not contribute to the PSF centroiding of the primary star.

We measure the location of 5B in the 2009 April 11 and 2009 June 9 epochs, which both had excellent seeing of $\sim 0''.7$. Because we were integrating on TWA 5A in the GW at 0.2 s and the reference FF for 30 s or 12 s, respectively, we have 2250 (720) GW images to use for “lucky imaging” to select the best few hundred images on each date. For each epoch, we shift and add these on the brightest pixel to form a final image with high quality – FWHM of $0''.54$ on 11 April and $0''.60$ on 9 June. In these images, we measure the separation and position angles of the brown dwarf 5B with respect to 5A. The location of 5A is well-determined by the shift-and-add process. To find the TWA 5B centroid, we examine individually the flux in slices of each row and column around its location. In each slice, we subtract a smooth continuum from the bright star, and then fit the peak produced by 5B with a Gaussian. We then average the individual slice locations weighted by the height of the Gaussian in each slice to produce separate centroids in RA and DEC. Unfortunately, TWA 5B falls nearly on top of a diffraction spike that limits our ability to accurately centroid. The average separation on the two dates is $2''.00 \pm 0''.10$.

We use 2MASS sources in the larger astrometric frame to solve for any PA offset between CAPSCam and the 2MASS reference frame and find offsets of 0.17 and 0.22 deg on the two dates. A match of the CAPSCam and 2MASS fields is also used to measure the CAPSCam pixel scale

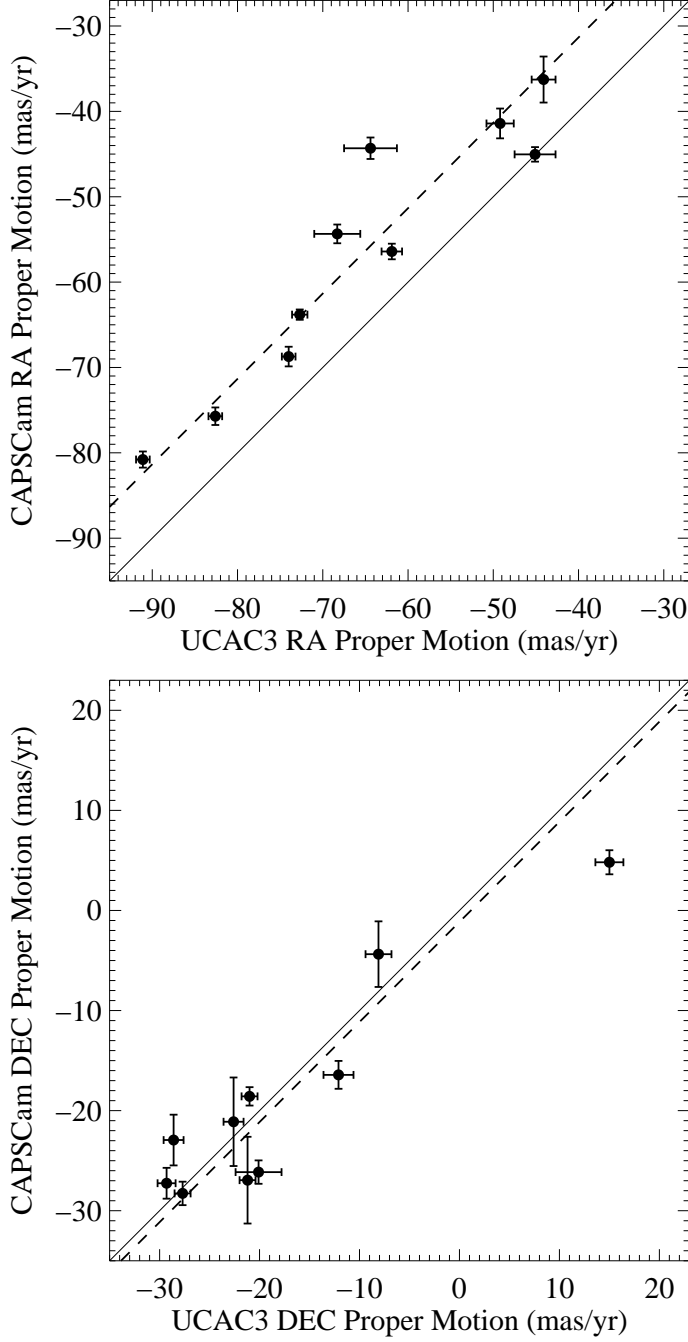


Fig. 1.— Comparison of proper motions of the ten TWA stars both reported in UCAC3 (Zacharias et al. 2009) and measured in our survey. The dashed lines show the mean offsets of 8.8 mas/yr in RA and -1.1 mas/yr in DEC between our relative proper motions and the absolute UCAC3 ones.

of 0.1958 ± 0.0005 arcsec pixel⁻¹. The average position angle of B with respect to A in the 2009 epochs is 358.3 ± 2.0 degrees. Both the separation and position angle are consistent with the measurements of Neuhauser et al. (2010) taken one year earlier.

TWA 5A itself is a binary whose orbit of period 6 yr was measured with AO imaging (Konopacky et al. 2007). We determine its distance to be 50.1 ± 1.8 pc. The total dynamical mass of the components from the astrometric orbit depends strongly on distance ($\propto D^3$), which was taken in Konopacky et al. to be 44 ± 4 pc from the convergent point analysis by Mamajek (2005). Our parallactic distance is a 14% change from the Mamajek estimate, which makes a significant change in the inferred dynamical mass. The mass is now estimated at $1.05 \pm 0.22 M_{\odot}$ instead of $0.71 \pm 0.14 M_{\odot}$.

When we correct the absolute magnitude of TWA 5A for binarity using $\Delta\text{mag} \approx 1.1$ at H-band as measured by Konopacky et al. (2007), we find that this brings the dynamical mass into good agreement with the Baraffe et al. (1998) pre-main sequence tracks, which predict a total mass of $1.2 M_{\odot}$ and an age of 10 ± 1 Myr from our interpolation in Section 4.1 (see also Figure 4 of Konopacky et al.).

This assumed that there were two and only two components in TWA 5A. However, there have been suggestions of additional rapid, high velocity variability that would suggest a separate spectroscopic binary within TWA 5Aa or 5Ab. (Torres et al. 2003) report that TWA 5A may be double-lined with possible day-scale velocity changes, but does not present individual RV measure-

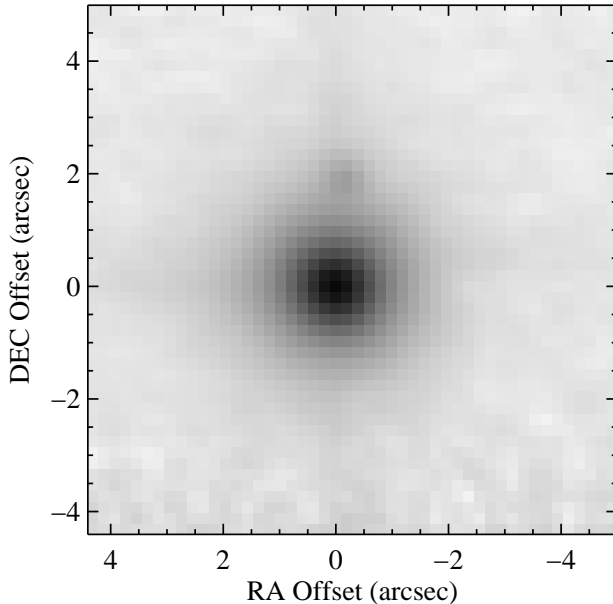


Fig. 2.— Image of TWA 5A and 5B from the sum of 782 individual 0.2 s images taken 2009 April 11 that were shifted to stack the brightest pixel at the center. TWA 5B is visible 2'' north of the primary.

ments. Reid (2003) find two components separated by 30 km s^{-1} , and may have observed the AO binary near periastron. Periastrons were in 1998.40, 2004.34, and 2010.28 according to the (Konopacky et al. 2007) ephemeris. Song et al. (2002) report a single velocity of $-30.6 \pm 6.6 \text{ km s}^{-1}$ measured in 2001-2002 at apastron. Other measurements find mean velocity of $\sim 13 \text{ km s}^{-1}$ with variability and line shapes consistent with motion of a few km s^{-1} (Torres et al. 2006, 2008; Shkolnik et al. 2011). TWA Aa and Ab are of very similar spectral type and brightness, and have significant rotational velocity $> 30 \text{ km s}^{-1}$ (Torres et al. 2003; Reid 2003), so their lines should be difficult to distinguish. The AO orbit predicts a maximum relative velocity of $\sim 18 \text{ km s}^{-1}$. If there is a third star within TWA 5A, then the age of TWA 5Aa/Ab from the (Baraffe et al. 1998) tracks would be underestimated (i.e. they would have lower luminosity). Their masses from the tracks would be essentially unchanged because the tracks are nearly vertical (see Figure 5), but the addition of the mass of the third component would imply that the tracks overestimate the dynamical masses of Aa/Ab alone.

3.1.2. TWA 11C

Kastner et al. (2008) identified 2M1235 as a likely tertiary companion to HR 4796A, ie. as TWA 11C. Its parallactic distance of $69.0 \pm 2.4 \text{ pc}$ indeed agrees well with the Hipparcos distance to HR 4796A of $72.8 \text{ pc} \pm 1.7 \text{ pc}$ (van Leeuwen 2007).

3.1.3. TWA 16

Zuckerman et al. (2001) reported that TWA 16 was a close visual binary with separation $\sim 0''.67$ and flux ratio ~ 0.9 . The CAPSCam images reveal an elongated source in all epochs and resolve two sources during the observations with the best seeing (Figure 3). The pipeline does not identify two sources there, however, so the measured parallax and proper motion are for the photocenter of the system. For the 2009 June 8 data, which had the best seeing, we used “lucky imaging” to select the best few hundred GW images. We shift and added these on the brightest pixel to form a final image with high quality and then used PSF fitting to measure the separation as $0''.61 \pm 0''.02$, PA as 44° , and flux ratio as 0.97.

4. Discussion

4.1. Pre-Main Sequence Track Ages

We determine absolute magnitudes using our parallaxes and 2MASS apparent magnitudes. We also correct for binarity for six sources. TWA 2 is a visual binary with $\Delta\text{mag} \approx 1$ (Webb et al. 1999). TWA 5A (see Section 3.1.1) is a close (speckle/AO resolved) binary with $\Delta\text{mag} \approx 1.1$ (Konopacky et al. 2007). TWA 14 is an approximately equal brightness SB (Jayawardhana et al. (2006) and Shkolnik, 2011, personal communication). TWA 16 is a visual binary with a flux ratio of 0.9 (Zuckerman et al. 2001). TWA 20 is a SB for which we assume the components are

equal brightness (Jayawardhana et al. 2006). TWA 23 is a SB with equal brightness components (Shkolnik et al. 2011). No attempt has been made to correct for extinction, which is small in the near-infrared due to the closeness of the stars and the absence of edge-on optically thick circumstellar disks in our sample. The tabulated uncertainties in absolute magnitude include the photometric uncertainty in the 2MASS H-band measurement and the parallax uncertainty.

We obtain effective temperatures by converting literature spectral types to temperature using the intermediate scale of Luhman (1999) for the M-type stars and tabulated values in Hartigan et al. (1994) for the earlier type stars. These are all given in Table 3. Most of the spectral types come from recent compilations that use TiO band or other spectral index fitting and should be mutually consistent and good to ~ 75 K. TWA 25 has no published spectral type; to obtain its temperature, we fit a Kurucz model to its photometry. TWA 29 (DEN1245) is the latest spectral type object for which we measured a parallax and sits near the M-L transition. The spectral-type to effective temperature conversion is not well known for such objects, and we approximate it at 2250 K. Finally, we must note that historical optical and new infrared spectral types for TW Hya do not agree (Webb et al. 1999; Vacca & Sandell 2011). TW Hya’s optical spectrum has been typed as K7V, 4000 K, but the Vacca & Sandell (2011) determination of 3400 K is likely to be too cool (N. Calvet, 2012, personal communication); we have chosen an intermediate value of the T_{eff} of 3615 K.

Theoretical isochrones overplotted with the data for all stars with parallaxes (literature as well as this work) are shown in Figure 4. We have chosen the Baraffe et al. (1998) tracks with $Y=0.775$,

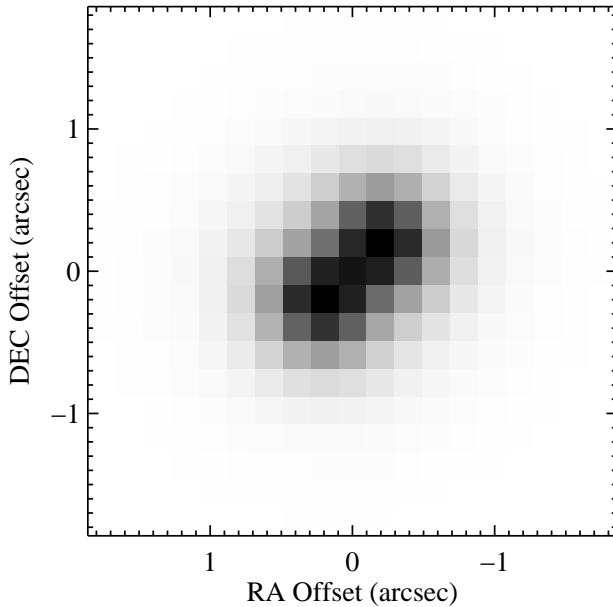


Fig. 3.— Image of the close binary TWA 16 on 2009 June 8 with a separation of $0''.61 \pm 0''.02$ and PA of 44° .

mixing length parameter 1 for $m < 0.6 M_{\odot}$ and $Y = 0.282$, mixing length 1.9 for $m \geq 0.6 M_{\odot}$, based on their relative success in reproducing multiple star coevality (White et al. 1999). The combination of the isochrones with different helium abundances creates a small temperature discontinuity at 3500-3700 K, which is unfortunately the temperature range of many of our stars (Table 3), but we interpolate over this region anyway. We use the DUSTY isochrones (Chabrier et al. 2000) for the stars with $T_{\text{eff}} < 2900$ K. We interpolate the combined theoretical tracks to estimate the ages of all the stars at their nominal positions in absolute magnitude- T_{eff} space. The median age is 10.1 Myr. Individual ages are also given in Table 3, along with all the data plotted on the tracks. Because of the abundance of stars with $T_{\text{eff}} \sim 3600$ K, Figure 5 shows a zoomed view of this part of the diagram. From the parallax uncertainty alone, the typical age uncertainty on each star is 3 Myr. An age of 10 Myr is consistent with previous estimates, as summarized in Fernández et al. (2008).

4.2. Galactic Space Motion and Membership

For the analysis of the kinematics of the group, we use all stars with known proper motions (from UCAC3 if available), parallaxes, and radial velocities. These are given along with calculated UVWs in Table 4. Uncertainties in all three quantities are propagated into the final velocity uncertainties. We also use positions from the 2MASS catalog (Skrutskie et al. 2006). We then compute the mean velocity of the entire TW Hya association.

The uncertainty weighted average velocities in Table 4 are $[-10.1, -17.9, -8.0] \pm [0.2, 0.2, 0.1]$ km s $^{-1}$. Two stars have velocities more than 3σ from the mean of the association in at least two directions: TWA 9A and TWA 22. TWA 22 was already suspected not to be a member by Mamajek (2005) and Teixeira et al. (2009), based on similar velocity arguments. However, TWA 9A is a “classical” member used to define the convergent point in the Mamajek analysis. Given its discrepant age in Table 3, as well as its discrepant velocity, we conclude it is not a member or that its Hipparcos distance is underestimated. The new average velocities after excluding these two stars are: $[-10.9, -18.2, -5.3] \pm [0.2, 0.2, 0.2]$ km s $^{-1}$. The standard deviation of the total velocities is 2.0 km s $^{-1}$, and the RMS deviation in the total velocity from the mean total velocity is 1.9 km s $^{-1}$. These are considerably lower dispersions than obtained when photometric distances are used (Fernández et al. 2008).

The uncertainties on the mean velocities above are computed assuming the stellar velocity distribution is Gaussian, i.e. standard deviation of velocities divided by the square-root of the number of stars. However, a K-S test reveals that the velocities are not Gaussianly distributed. Nor are they uniformly distributed between their minimum and maximum values.

To trace the stars back in time, we take their present positions and three-dimensional space velocities and compute their locations in Galactic coordinates for time-steps back every 100,000 years. To treat the distance and velocity uncertainties properly, we do this in a Monte Carlo for 10000 trials selecting each star’s distance and velocity in each direction randomly in each trial but distributed assuming the uncertainties for each individual star are Gaussian. Then, the centroid 3D location of the stars at each time is computed as well as the average distance of the stars from this centroid. The time of best convergence is defined to be when the average distance is minimized. We

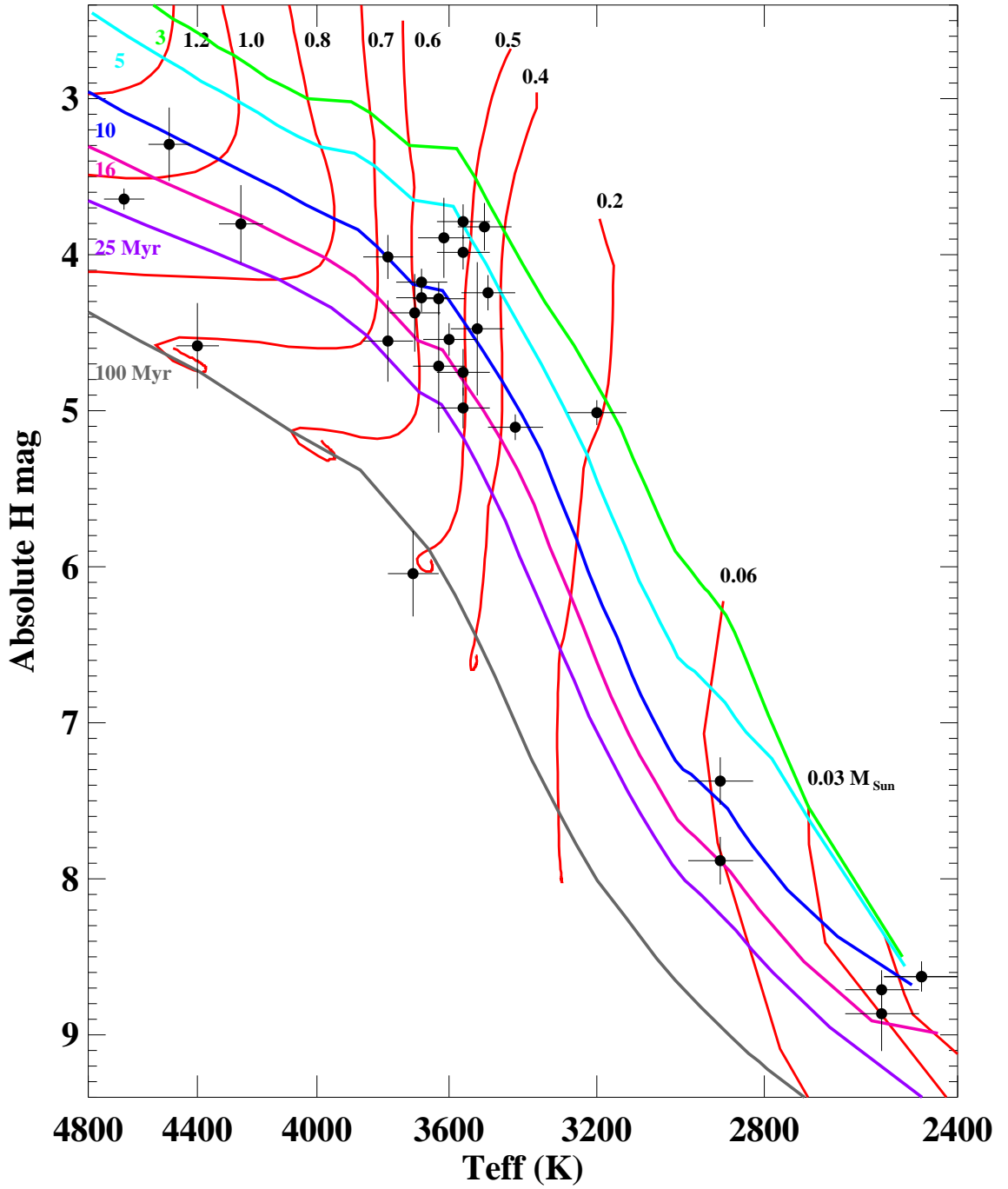


Fig. 4.— TWA stars with parallaxes, and therefore absolute magnitudes, plotted on theoretical pre-main sequence tracks from Baraffe et al. (1998) and Chabrier et al. (2000). Effective temperatures largely come from converting published spectral types to temperature and have uncertainties (as shown) of at ~ 75 K (one half of a spectral type). The apparent scatter in ages is discussed in section 4.1 and Fig. 8.

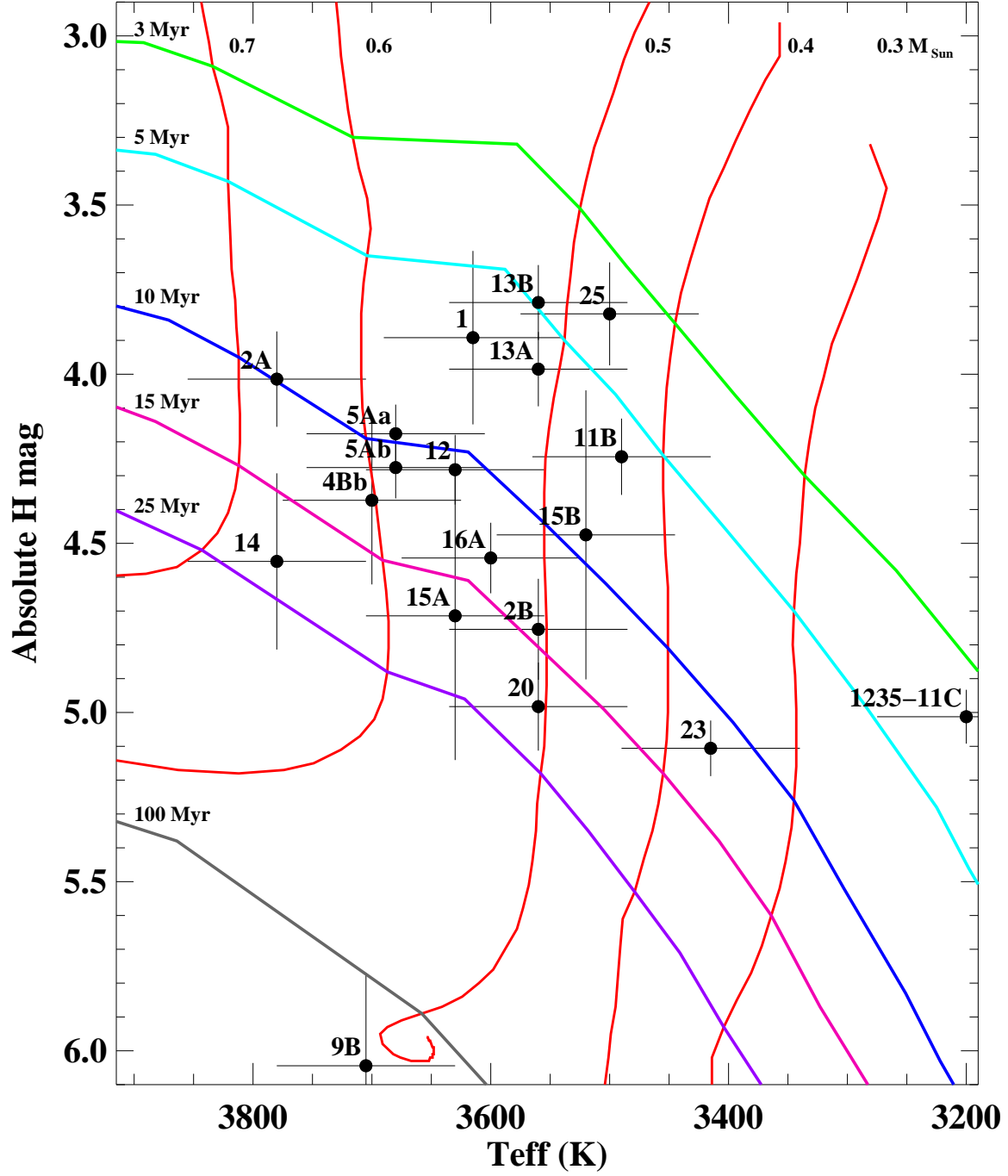


Fig. 5.— Closeup of Figure 4 in the region around $T_{\text{eff}}=3600$ K where most of the stars sit.

tested that the Galactic potential does not significantly affect the motions over the short timescale of 10 Myr.

The present average distance from their mean location for the stars in Table 4, excluding 9A and 22, is 20.4 pc. The present-day locations of the TWA stars with measured parallaxes and radial velocities is shown in Figure 6. The velocities are nearly parallel, as shown in Figure 7. The nominal closest approach of all the stars is 2 Myr ago, but has a mean distance of 19.2 pc from the center, meaning that there is no time in the past when the stars are significantly more concentrated than they are today. At the mean age of 10 Myr established in section 4.1, the mean distance from the center is 34 pc.

Figure 8 displays a histogram of the ages excluding 9AB, 22, and 29. There is a tail of stars to apparently larger ages while there are no stars with inferred ages less than 3 Myr. The best Gaussian fit to the age distribution has a mean of 9.5 Myr and standard deviation of 5.7 Myr. To assess the reliability of these values for such a small sample, we repeated the histogram fit in a Monte Carlo. In each trial, the age of each star was drawn from a Gaussian distribution based on that individual’s star mean age and absolute magnitude uncertainty on the Baraffe et al. (1998) tracks. The typical age uncertainty on each star is 3 Myr. The mean age over all the trials was 8.7 Myr and the width of the age distribution over all the trials was 6.5 Myr. Thus, the age histogram is robust against the individual age uncertainties, and the width of the distribution compared to the typical age uncertainty indicates that there is a real spread in derived ages.

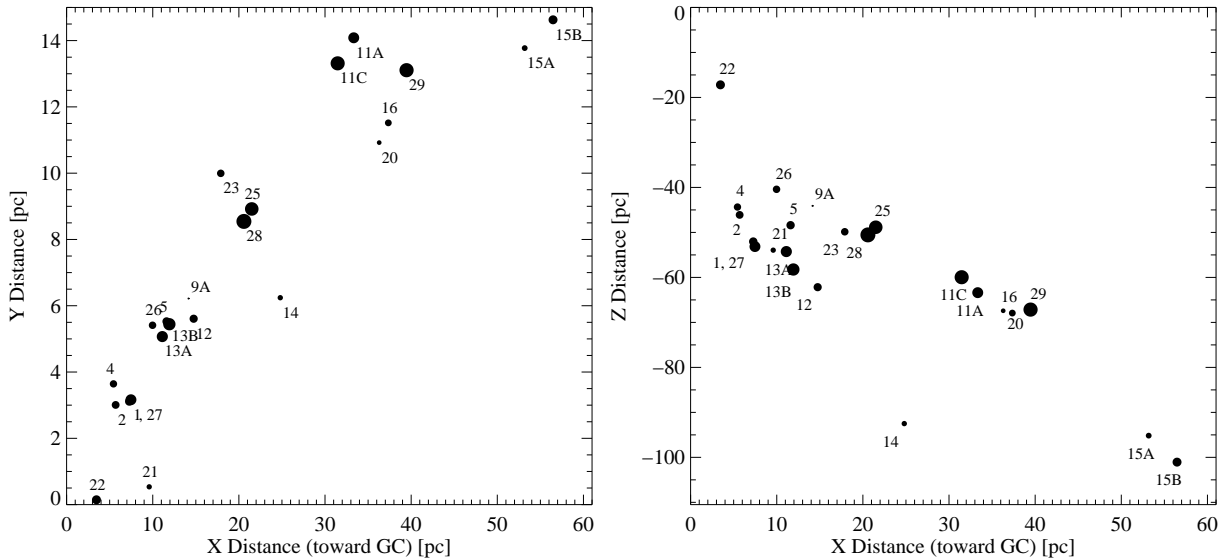


Fig. 6.— Location of the TWA stars currently in Galactic coordinates. The size of the symbols is inversely proportional to age; that is, larger symbols indicate younger stars, as determined in Section 4.1. There is no apparent correlation between age and location.

5. Conclusions

The identification of TWA members has largely been based on youth plus similarity to the young star TW Hya in terms of location on the sky, proper motion, and radial velocity. Co-evality was thought to follow under the assumption that these stars with similar motions formed from the same raw material at the same time. With parallaxes to fourteen primary stars identified as TWA members, we have greatly expanded the knowledge of the kinematics of these young stars. We find that although they do share a common space motion, the stars do not appear to have formed in a concentrated volume with a well-defined expansion velocity. The TWA stars appear to have formed over a larger volume than they presently occupy.

Nor do the stars appear to be completely co-eval, as the stars studied here have ages that range from 3–23 Myr as derived from their locations on pre-main sequence tracks. Although uncertainties in the distance and the effective temperatures allow for several Myr of uncertainty in individual ages, it would be extremely difficult to force them all to a common age. This apparent age spread could be due to a real difference in the times of formation of the stars or it could be due to the lasting effects of episodic accretion (Baraffe et al. 2009).

The spatial distribution of these nominal TWA stars of 40–60 pc is largely filamentary in nature, which naturally leads to some conclusions about their provenance. Perhaps the stars formed in an extended wisp of molecular cloud, probably one related to the Scorpius-Centaurus complex that is nearby on the sky but 80 pc further away. The Galactic V and W velocities of TWA are very similar to the older Upper Centaurus Lupus (UCL) and Lower Centaurus Crux (LCC) subgroups of Sco-Cen (Chen et al. 2011) at ages of 15–17 Myr (Mamajek et al. 2002). TWA is located near to LCC in Galactic coordinates but their separation in distance, age, and velocity distinguish the two

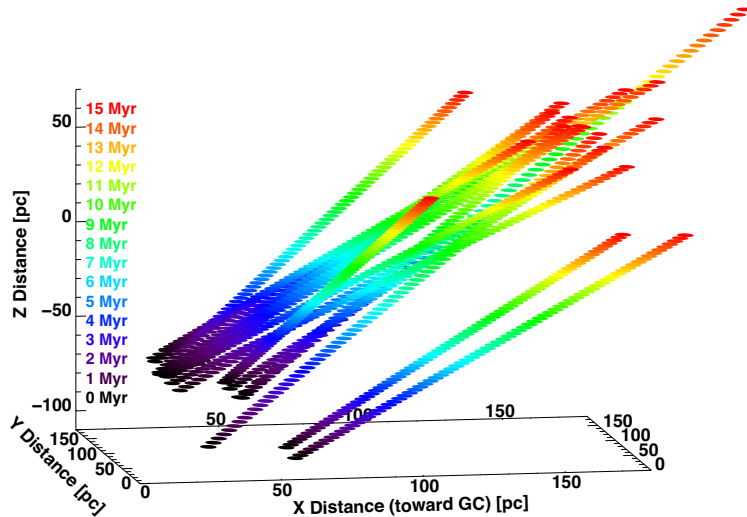


Fig. 7.— Three-dimensional space motion of the TWA stars with measured parallaxes and radial velocities in Galactic coordinates. Black dots show the present locations of the stars and the colored points show the motion in 200,000 yr timesteps for 15 Myr. The parallel velocities mean that the stars are never much closer together than they are at present. This plot excludes TWA 9A and 22.

groups. Fernández et al. (2008) showed that TWA was *sim*45 pc from LCC 8 Myr ago and could have been subjected to 0.5 supernovae per Myr. Multiple supernova shocks could have triggered star formation in dense parts of the filamentary progenitor TWA cloud over a few million years and not in a regular progression from one side to the other. (Ortega et al. 2009) also suggest that stellar winds and supernovae from LCC and UCL could compress gas in the region of TWA, although the mechanism for an extended time of star formation is less clear in this case.

The Las Campanas Observatory staff and operators of the duPont telescope, particularly Oscar Duhalde, Javier Fuentes, Herman Oliveras, Patricio Pinto, and Andrés Rivera, made the CAPSCam observations smooth and efficient. Rebecca Rattray made helpful analyses of portions of these TWA data during an undergraduate internship at DTM in 2009. CAPSCam was built with support from the NSF ATI program and Carnegie Institution of Washington. We acknowledge support for the observing by the NASA Astrobiology Institute under cooperative agreement NNA09DA81A.

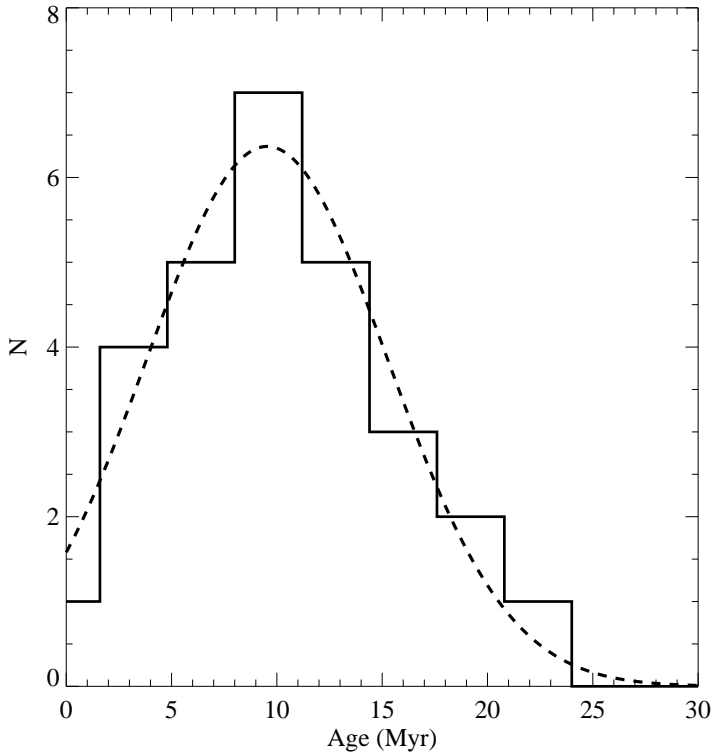


Fig. 8.— Age histogram of the TWA stars with parallaxes, excluding 9AB and 22, which have kinematics inconsistent with membership, and 29, which has a highly uncertain T_{eff} and therefore uncertain age. The bin size is 3 Myr, which is the median uncertainty in the individual ages based on the uncertainties in their absolute magnitudes (i.e., parallaxes). The best fit Gaussian to the age distribution is overplotted with the dashed line and has a mean of 9 Myr and standard deviation of 6.8 Myr. The width of the age distribution exceeds what would be expected for a population of stars formed in a single burst.

This work makes use of the Simbad database and VizieR catalogue access tool, CDS, Strasbourg, France, and the 2MASS survey, which is a joint project of the University of Massachusetts and the Infrared Processing and Analysis Center/California Institute of Technology, funded by the National Aeronautics and Space Administration and the National Science Foundation.

REFERENCES

- Anglada-Escudé, G., Boss, A. P., Weinberger, A. J., et al. 2012, *ApJ*, 746, 37
- Baraffe, I., Chabrier, G., Allard, F., & Hauschildt, P. H. 1998, *A&A*, 337, 403
- Baraffe, I., Chabrier, G., & Gallardo, J. 2009, *ApJ*, 702, L27
- Barrado Y Navascués, D. 2006, *A&A*, 459, 511
- Biller, B. A., & Close, L. M. 2007, *ApJ*, 669, L41
- Bonnefoy, M., Chauvin, G., Dumas, C., et al. 2009, *A&A*, 506, 799
- Boss, A. P., Weinberger, A. J., Anglada-Escudé, G., et al. 2009, *PASP*, 121, 1218
- Chabrier, G., Baraffe, I., Allard, F., & Hauschildt, P. 2000, *ApJ*, 542, 464
- Chen, C. H., Mamajek, E. E., Bitner, M. A., et al. 2011, *ApJ*, 738, 122
- de la Reza, R., Torres, C. A. O., Quast, G., Castilho, B. V., & Vieira, G. L. 1989, *ApJ*, 343, L61
- Ducourant, C., Teixeira, R., Chauvin, G., et al. 2008, *A&A*, 477, L1
- Fernández, D., Figueras, F., & Torra, J. 2008, *A&A*, 480, 735
- Gizis, J. E. 2002, *ApJ*, 575, 484
- Gizis, J. E., Jao, W.-C., Subasavage, J. P., & Henry, T. J. 2007, *ApJ*, 669, L45
- Gregorio-Hetem, J., Lepine, J. R. D., Quast, G. R., Torres, C. A. O., & de la Reza, R. 1992, *AJ*, 103, 549
- Hartigan, P., Strom, K. M., & Strom, S. E. 1994, *ApJ*, 427, 961
- Jayawardhana, R., Coffey, J., Scholz, A., Brandeker, A., & van Kerkwijk, M. H. 2006, *ApJ*, 648, 1206
- Kastner, J. H., Zuckerman, B., & Bessell, M. 2008, *A&A*, 491, 829
- Kastner, J. H., Zuckerman, B., Weintraub, D. A., & Forveille, T. 1997, *Science*, 277, 67
- Konopacky, Q. M., Ghez, A. M., Duchêne, G., McCabe, C., & Macintosh, B. A. 2007, *AJ*, 133, 2008
- Looper, D. L., Burgasser, A. J., Kirkpatrick, J. D., & Swift, B. J. 2007, *ApJ*, 669, L97

- Looper, D. L., Mohanty, S., Bochanski, J. J., et al. 2010, *ApJ*, 714, 45
- Low, F. J., Smith, P. S., Werner, M., et al. 2005, *ApJ*, 631, 1170
- Luhman, K. L. 1999, *ApJ*, 525, 466
- Makarov, V. V., & Fabricius, C. 2001, *A&A*, 368, 866
- Mamajek, E. E. 2005, *ApJ*, 634, 1385
- Mamajek, E. E., Meyer, M. R., & Liebert, J. 2002, *AJ*, 124, 1670
- Mohanty, S., Jayawardhana, R., & Barrado Y Navascués, D. 2003, *ApJ*, 593, L109
- Mohanty, S., Jayawardhana, R., Huélamo, N., & Mamajek, E. 2007, *ApJ*, 657, 1064
- Monet, D. G., Levine, S. E., Canzian, B., et al. 2003, *AJ*, 125, 984
- Neuhäuser, R., Schmidt, T. O. B., Hambaryan, V. V., & Vogt, N. 2010, *A&A*, 516, 112
- Ortega, V. G., Jilinski, E., de la Reza, R., & Bazzanella, B. 2009, *AJ*, 137, 3922
- Plavchan, P., Werner, M. W., Chen, C. H., et al. 2009, *ApJ*, 698, 1068
- Prato, L., Ghez, A. M., Piña, R. K., et al. 2001, *ApJ*, 549, 590
- Reid, N. 2003, *Monthly Notice of the Royal Astronomical Society*, 342, 837
- Riaz, B., & Gizis, J. E. 2008, *ApJ*, 681, 1584
- Rucinski, S. M., & Krautter, J. 1983, *A&A*, 121, 217
- Schneider, A., Melis, C., & Song, I. 2012, *ApJ*, 754, 39
- Scholz, R.-D., McCaughrean, M. J., Zinnecker, H., & Lodieu, N. 2005, *A&A*, 430, L49
- Shkolnik, E. L., Liu, M. C., Reid, I. N., Dupuy, T., & Weinberger, A. J. 2011, *ApJ*, 727, 6
- Skrutskie, M. F., Cutri, R. M., Stiening, R., et al. 2006, *AJ*, 131, 1163
- Soderblom, D. R., King, J. R., Siess, L., et al. 1998, *ApJ*, 498, 385
- Song, I., Bessell, M. S., & Zuckerman, B. 2002, *A&A*, 385, 862
- Song, I., Zuckerman, B., & Bessell, M. S. 2003, *ApJ*, 599, 342
- Stauffer, J. R., Hartmann, L. W., & Barrado Y Navascués, D. 1995, *ApJ*, 454, 910
- Sterzik, M. F., Alcalá, J. M., Covino, E., & Petr, M. G. 1999, *A&A*, 346, L41
- Teixeira, R., Ducourant, C., Chauvin, G., et al. 2009, *A&A*, 503, 281
- . 2008, *A&A*, 489, 825

- Torres, C., Quast, G., Melo, C., & Sterzik, M. 2008, in *Handbook of Star Forming Regions, Volume II: The Southern Sky*, ed. B. Reipurth, ASP Monograph Publications Vol. 5 (San Francisco, CA: ASP), 757–812
- Torres, C. A. O., Quast, G. R., da Silva, L., et al. 2006, *A&A*, 460, 695
- Torres, G., Guenther, E. W., Marschall, L. A., et al. 2003, *AJ*, 125, 825
- Vacca, W. D., & Sandell, G. 2011, *ApJ*, 732, 8
- van Leeuwen, F. 2007, *Hipparcos, the New Reduction of the Raw Data*, Astrophysics and Space Science Library Vol. 350 (Springer)
- Webb, R. A., Zuckerman, B., Platais, I., et al. 1999, *ApJ*, 512, L63
- Weinberger, A. J., Becklin, E. E., Zuckerman, B., & Song, I. 2004, *AJ*, 127, 2246
- White, R. J., Ghez, A. M., Reid, I. N., & Schultz, G. 1999, *ApJ*, 520, 811
- Zacharias, N., Finch, C., Girard, T., et al. 2009, *VizieR On-line Data Catalog*, 1315, 0
- Zuckerman, B., & Song, I. 2004, *ARAA*, 42, 685
- Zuckerman, B., Webb, R. A., Schwartz, M., & Becklin, E. E. 2001, *ApJ*, 549, L233

Table 1. Observation Log

Target	Other Name	I (mag)	Ref	Integration Times		Epochs of Observation (JD)
				GW (s)	FF (s)	
TWA 2		8.9	1,2	0.2	40	2454167.7, 2454809.8, 2454818.8, 2454931.7, 2454989.5, 2454992.5, 2455222.8, 2455295.9, 2455297.9, 2455369.6
TWA 5		9.3	5	0.2	12	2454664.5, 2454810.8, 2454932.7, 2454990.4, 2454991.5, 2455222.9, 2455368.7, 2455579.9
TWA 11C	2M1235-39	11.2	2	–	30	2454861.8, 2454929.6, 2454989.6, 2454992.5, 2455224.8, 2455369.7
TWA 12		10.5	5	0.6	20	2454167.7, 2454168.1, 2454663.4, 2454809.8, 2454859.8, 2454932.7, 2454991.5, 2455222.9
TWA 13		10.1/10.1	3	0.5	20	2454810.8, 2454859.8, 2454930.7, 2454988.5, 2455218.8
TWA 14		10.7	5	0.5	20	2454810.8, 2454859.7, 2454929.8, 2454986.5, 2455218.8
TWA 15		11.8/11.9	4	1.0	45	2454813.8, 2454930.7, 2454990.5, 2455219.8, 2455636.8
TWA 16		10.2	4	1.0	30	2454861.8, 2454929.7, 2454988.5, 2454989.5, 2454991.5, 2455219.9
TWA 20		10.7	5	1.0	30	2454859.8, 2454929.7, 2454987.5, 2455223.9
TWA 21		9.0	5	0.2	30	2454813.7, 2454929.6, 2454985.5, 2455216.8, 2455297.9, 2455370.6
TWA 23		10.1	5	0.5	60	2454168.7, 2454291.5, 2454661.5, 2454811.8, 2454852.8, 2454861.8, 2454989.5, 2454992.4
TWA 25		9.5	1	0.3	45	2454168.3, 2454291.5, 2454663.5, 2454861.8, 2454991.5, 2455299.1
TWA 26	2M1139-31	15.8	5	–	30	2454809.1, 2454930.7, 2454985.5, 2455217.8, 2455295.9, 2455584.1
TWA 29	DEN1245-44	18.0	5	–	60	2454861.7, 2454990.6, 2455217.9, 2455368.7, 2455410.1

^aI-band magnitudes are from (1) USNOB1.0 (Vizier I/284; (Monet et al. 2003)), (2) UCAC3 (Vizier I/315), (3) Reid (2003), (4) Zuckerman et al. (2001) or (5) DENIS (Vizier B/denis)

Table 2. Astrometric Results

Target	π_{rel}	$\mu_{RA \cos DEC, rel}$	$\mu_{DEC, rel}$	Zero-point	π_{abs}
TWA 2	21.76 ± 1.26	-80.8 ± 0.9	-18.6 ± 0.9	0.28 ± 0.30	21.48 ± 1.30
TWA 5	20.07 ± 0.67	-75.7 ± 1.0	-21.1 ± 4.4	0.10 ± 0.19	19.97 ± 0.70
TWA 11C	14.55 ± 0.38	-45.0 ± 0.8	-26.1 ± 1.2	0.06 ± 0.34	14.49 ± 0.51
TWA 12	15.43 ± 0.59	-54.4 ± 1.1	-16.4 ± 1.4	-0.16 ± 0.37	15.59 ± 0.70
TWA 13A (NW)	17.89 ± 0.68	-57.7 ± 1.7	-13.6 ± 0.9	-0.09 ± 0.23	17.98 ± 0.72
TWA 13B (SE)	16.66 ± 0.70	-59.3 ± 2.6	-12.2 ± 2.1	-0.09 ± 0.23	16.75 ± 0.74
TWA 14	10.15 ± 1.19	-36.3 ± 2.7	-4.4 ± 3.3	-0.27 ± 0.21	10.42 ± 1.21
TWA 15A (NE)	8.27 ± 1.61	-28.8 ± 1.6	-11.5 ± 1.2	-0.30 ± 0.13	8.57 ± 1.62
TWA 15B (SW)	8.80 ± 1.72	-27.8 ± 2.3	-11.0 ± 2.3	-0.30 ± 0.13	9.10 ± 1.72
TWA 16	13.04 ± 0.49	-41.4 ± 1.7	-26.9 ± 4.3	0.28 ± 0.12	12.76 ± 0.50
TWA 20	12.85 ± 0.59	-44.3 ± 1.2	-22.9 ± 2.5	-0.08 ± 0.15	12.93 ± 0.61
TWA 21	18.20 ± 0.46	-56.4 ± 0.9	4.8 ± 1.2	-0.05 ± 0.17	18.25 ± 0.49
TWA 23	18.41 ± 0.33	-63.8 ± 0.6	-27.2 ± 1.5	-0.14 ± 0.35	18.55 ± 0.48
TWA 25	18.39 ± 1.23	-68.7 ± 1.2	-28.3 ± 1.2	-0.09 ± 0.14	18.48 ± 1.24
TWA 26	23.38 ± 2.54	-81.2 ± 3.9	-27.7 ± 2.1	-0.44 ± 0.46	23.82 ± 2.58
TWA 29	12.61 ± 2.06	-40.3 ± 11.7	-20.3 ± 17.0	-0.05 ± 0.18	12.66 ± 2.07

Table 3. Stellar Parameters

Star	Sp. Type	Sp. Type Ref	Teff	H(abs)	H unc	BCAH98 age
1	K7.0	Webb et al. (1999)	3615	3.91	0.26	6
2A	M0.5	Webb et al. (1999)	3780	4.03	0.14	9
2B	M2	Webb et al. (1999)	3560	4.77	0.15	17
4Aab	K4.0	Prato et al. (2001)	4500	3.31	0.24	11
4Ba	K4.0	Soderblom et al. (1998)	4250	3.82	0.25	15
4Bb	K4.0	Soderblom et al. (1998)	3700	4.39	0.25	12
5A	M1.5	Konopacky et al. (2007)	3680	4.19	0.09	9
5B	M8.5	Konopacky et al. (2007)	3680	4.29	0.09	11
9A	K5.0	Webb et al. (1999)	4400	4.60	0.27	63
9B	M1.0	Webb et al. (1999)	3705	6.06	0.27	150
11B	M2.5	Webb et al. (1999)	3490	4.26	0.11	6
11C	M4.5	Kastner et al. (2008)	3200	5.03	0.08	4
12	M1.6	Shkolnik et al. (2011)	3630	4.30	0.10	10
13A	M2.0	Sterzik et al. (1999)	3560	4.00	0.11	6
13B	M2.0	Sterzik et al. (1999)	3560	3.80	0.11	5
14	M0.6	Shkolnik et al. (2011)	3780	4.57	0.26	19
15A	M1.5	Zuckerman et al. (2001)	3630	4.73	0.43	17
15B	M2.2	Shkolnik et al. (2011)	3520	4.49	0.43	9
16A	M1.8	Shkolnik et al. (2011)	3600	4.56	0.10	14
20	M2.0	Reid (2003)	3560	5.00	0.13	23
21	K3.5	Zuckerman & Song (2004)	4665	3.66	0.07	19
22A	M6.0	Bonnefoy et al. (2009)	2900	7.39	0.15	6
22B	M6.0	Bonnefoy et al. (2009)	2900	7.90	0.15	12
23	M2.9	Shkolnik et al. (2011)	3415	5.12	0.08	12
25	M2.0	color	3500	3.84	0.15	4
26	M8.0	Mohanty et al. (2003)	2550	8.88	0.24	12
27	M8.0	Mohanty et al. (2007)	2550	8.73	0.12	10
28	M8.5	Scholz et al. (2005)	2470	8.64	0.06	3
29	M9.5	Looper et al. (2007)	2250	9.31	0.37	4

Table 4. Velocities

Star	π (mas)	$\sigma\pi$ (mas)	$\mu_{RA \cos DEC}$ (mas yr ⁻¹)	μ_{DEC} (mas yr ⁻¹)	$\sigma\mu_{RA}$ (mas yr ⁻¹)	$\sigma\mu_{DEC}$ (mas yr ⁻¹)	RV (km s ⁻¹)	σ RV (km s ⁻¹)	U (km s ⁻¹)	σ U (km s ⁻¹)	V (km s ⁻¹)	σ V (km s ⁻¹)	W (km s ⁻¹)	σ W (km s ⁻¹)
1	18.6 ^a	2.1	-70.2	-13.7	2.5	1.1	12.7 ^d	0.2	-11.9	1.8	-18.0	0.7	-5.2	1.0
2	21.5	1.3	-91.1	-21.0	0.8	0.8	11.0 ^d	0.1	-13.8	1.1	-17.8	0.4	-6.3	0.5
4	22.3 ^a	2.3	-91.7	-28.2	1.5	2.4	9.2 ^d	1.0	-13.0	1.8	-17.2	0.9	-6.0	1.0
5	20.0	0.7	-82.6	-22.6	0.8	1.0	13.3 ^e	2.0	-11.8	0.8	-20.7	1.8	-4.8	0.9
9A	21.4 ^a	2.5	-53.1	-20.0	1.9	3.4	9.5 ^d	0.4	-5.7	1.3	-14.4	0.7	-2.9	0.9
11A	13.7 ^a	0.3	-53.3	-21.2	3.0	4.0	6.9 ^f	1.0	-10.8	1.1	-17.3	1.1	-5.2	1.3
11C	14.5	0.5	-45.1	-20.1	2.4	2.3	9 ^g	1.0	-6.8	0.9	-16.8	1.0	-3.4	0.8
12	15.6	0.7	-68.3	-12.1	2.7	1.5	13.1 ^e	1.6	-13.4	1.2	-20.1	1.5	-5.6	0.8
13A	18.0	0.7	-66.4	-12.5	2.4	1.8	11.7 ^d	0.6	-11.4	0.9	-17.6	0.6	-3.9	0.6
13B	16.8	0.7	-68.0	-11.0	3.1	2.7	12.6 ^d	0.5	-12.8	1.1	-18.9	0.7	-4.0	0.8
14	10.4	1.2	-44.1	-8.1	1.4	1.3	15.8 ^e	2.0	-11.7	2.2	-21.9	2.0	-6.8	1.2
15A	9.1	1.7	-37.5	-10.4	2.4	2.0	11.2 ^h	2.0	-10.3	3.6	-20.4	2.7	-3.7	1.5
15B	8.6	1.6	-36.5	-9.9	2.9	2.8	10.0 ^e	1.7	-11.4	3.8	-19.8	2.6	-4.1	1.9
16	12.8	0.5	-49.2	-21.2	1.6	0.8	9.0 ^e	0.4	-9.7	0.8	-18.6	0.6	-6.0	0.4
20	12.9	0.6	-64.4	-28.6	3.1	1.0	8.1 ^h	4.0	-14.2	2.3	-21.0	3.4	-9.5	1.3
21	18.2	0.5	-61.9	15.0	1.2	1.4	17.5 ⁱ	0.8	-12.0	0.5	-20.2	0.8	-4.9	0.4
22	57.0 ^b	0.7	-175.8	-21.3	0.8	0.8	14.8 ^b	2.1	-8.0	0.4	-17.1	2.0	-9.0	0.1
23	18.6	0.5	-72.7	-29.3	0.9	0.9	8.5 ^e	1.2	-10.6	0.6	-18.2	1.0	-5.4	0.6
25	18.5	1.2	-74.0	-27.7	0.8	0.8	9.2 ⁱ	2.1	-10.7	1.4	-18.7	1.9	-5.6	1.0
26	23.8	2.6	-89.9	-26.5	4.2	2.6	11.6 ^j	2.0	-10.7	2.0	-18.8	1.9	-3.8	1.3
27	19.0 ^c	0.4	-62.7	-22.8	1.7	2.8	11.2 ^j	2.0	-9.1	0.6	-16.6	1.8	-6.7	1.0

Note. — Parallaxes are from this work unless otherwise noted in footnotes. Sources of RVs are given in footnotes.

^aHipparcos – van Leeuwen (2007)

^bTeixeira et al. (2008)

^cWeighted average of Biller & Close (2007), Gizis et al. (2007), and Ducourant et al. (2008)

^dTorres et al. (2003)

^eShkolnik et al. (2011)

^fBright Star Catalog V/50

^gAssume same RV as for HR 4796B from Stauffer et al. (1995)

^hReid (2003)

ⁱSong et al. (2003)

ⁱMohanty et al. (2003)